

## Coupled dynamics of short waves and the airflow over long surface waves

V. N. Kudryavtsev<sup>1</sup>

Remote Sensing Department, Marine Hydrophysical Institute, Sevastopol, Ukraine

V. K. Makin

Observations and Modelling Department, Royal Netherlands Meteorological Institute, De Bilt, Netherlands

Received 10 December 2001; revised 1 July 2002; accepted 2 July 2002; published 3 December 2002.

[1] A study is presented of modulations induced by a dominant long surface wave (LW) in the coupled airflow–short wind-generated waves (SW) system. The modulation of SWs in the gravity range results from their interaction with the LW orbital velocity and their interaction with the wind stress modulated by the LW. The modulation of waves in the capillary range is mainly due to the modulation of the rate of generation of parasitic capillaries by steep short gravity waves. The variation of the wind surface stress is described by the dynamics of the turbulent airflow over the LW with the surface roughness varying along its profile. The variation of the surface roughness is caused by the variation of the form drag supported by modulated SWs. In turn, the LW-induced variation of the surface stress affects the SW modulation. This provides a feedback in the coupled airflow–SW system in the presence of the LW. The model results show that the amplitude of the surface roughness modulation can be large. In terms of the modulation transfer function (MTF), it can reach values of 10–20. The modulation of the form drag, which causes the modulation of the surface roughness, comes mainly from short breaking waves strongly modulated by dominant waves. The modulation of the surface roughness considerably affects the dynamics of the airflow over the LW and thus the LW wind growth rate. Models of the airflow above waves assuming a constant roughness parameter underestimate the growth rate parameter approximately two to three times as compared to the measured values. The present study shows that when the variation in the surface roughness is accounted for, the growth rate parameter increases roughly twice, which to a large extent reduces the discrepancy with measurements. *INDEX TERMS:* 4504

Oceanography: Physical: Air/sea interactions (0312); 4560 Oceanography: Physical: Surface waves and tides (1255); 3339 Meteorology and Atmospheric Dynamics: Ocean/atmosphere interactions (0312, 4504); 3307 Meteorology and Atmospheric Dynamics: Boundary layer processes; *KEYWORDS:* Short wind waves, modulation, wind-over-waves coupling, wave growth rate, radar modulation transfer function

**Citation:** Kudryavtsev, V. N., and V. K. Makin, Coupled dynamics of short waves and the airflow over long surface waves, *J. Geophys. Res.*, 107(C12), 3209, doi:10.1029/2001JC001251, 2002.

### 1. Introduction

[2] Dominant long surface waves (LWs) modulate short wind-generated waves (SWs), a phenomenon that is almost always present on the sea surface. The study of this problem has important applications. The modulation of SWs determines the hydrodynamic component of the wave radar modulation transfer function (MTF). Despite numerous efforts mechanisms responsible for the SW modulation are still poorly known. A traditional approach to model the SW modulation is based on the relaxation theory proposed by

*Alpers and Hasselmann* [1978]. However, applying this approach to reproduce observations led in most cases to failure [e.g., *Romeiser et al.*, 1994]. To reach agreement between model results and radar measurements *Hara and Plant* [1994] and *Romeiser et al.* [1994] assumed that the SW modulation is governed by a strong wave-induced surface stress variation with a maximum over the LW crest and amplitude of 10–20 times the LW steepness. No explanations for a mechanism providing such strong stress modulation was given. *Kudryavtsev et al.* [1997] developed a model, which takes into account the surface stress modulation resulting from a feedback between the airflow and the modulated SW. The general idea of this feedback is that areas of the surface with the enhanced SWs induce a large local wind stress due to the enhanced form drag. This stimulates the SW growth providing further enhancement of the SW energy.

<sup>1</sup>Also at Nansen Environmental and Remote Sensing Center, Bergen, Norway.

[3] The feedback mechanism suggested by *Kudryavtsev et al.* [1997] to explain the large amplitude of the LW-induced variation of the surface stress follows from a wind-over-wave coupling theory developed by *Makin et al.* [1995]. This theory was recently revised and extended to account for the impact of the airflow separation from breaking waves on the sea drag [*Kudryavtsev and Makin*, 2001]. It was shown that the airflow separation plays a crucial role in the formation of the sea drag under moderate and high wind speeds. *Dulov et al.* [2002] provided experimental evidence that wave breaking in the sea is strongly modulated by LWs. Hence, one can anticipate that the modulation in wave breaking should stimulate the modulation of the surface stress affecting the SW modulation.

[4] The goal of the present paper is to investigate the dynamics of the coupled system the airflow–SWs over a LW. The study is based on the background coupled sea surface–atmosphere model developed by *Kudryavtsev and Makin* [2001]. It is used here to describe the reaction of the coupled system the airflow–SWs in presence of a LW. The main attention is paid on the SW modulation (in the wavelength range from few millimeters to few meters), and on the variation of the surface stress and the aerodynamic roughness of the sea surface. The surface roughness varying along the profile of a LW can significantly affect the distribution of the surface pressure over the LW, and hence affects the growth rate of the LW [*Gent and Taylor*, 1976; *Maat and Makin*, 1992]. This effect can play a key role in better understanding of the wind wave generation problem. It is known [e.g., *Belcher and Hunt*, 1993; *Townsend*, 1972; *Mastenbroek et al.*, 1996] that models of the airflow above waves underestimate the growth rate parameter of waves as compared to empirical values. We show that accounting for the varying surface roughness significantly improves the agreement between the model and observed estimates of the growth rate parameter. Unlike previous studies the advantage of our approach is that the varying surface roughness is not specified arbitrarily but results from the solution of the coupled evolution of SWs and the turbulent airflow over longer surface waves.

## 2. Background

[5] In this section a brief overview of the background coupled sea surface–atmosphere model used to derive the modulation of SWs and the variation in the atmosphere parameters in presence of a LW is given. The background model consists of a model of the SW wave spectrum and the resistance law of the sea surface relating the drag of the sea surface to the wave spectrum. After the background model was fitted to measurements (e.g., the drag coefficient and the mean square slope) (Figure 1 below) it is used with the same tuning constants in the modulation problem (sections 3 and 4).

### 2.1. Energy Balance Equation and Wave Spectrum

[6] The form of the background spectrum of wind waves and its evolution in the nonuniform medium such as a surface current or wind results from a solution of the energy balance equation, which can be written in terms of the wave action spectral density  $N(\mathbf{k})$  [e.g., *Phillips*, 1977]

$$\frac{\partial N(\mathbf{k})}{\partial t} + (c_{gi} + u_i) \frac{\partial N(\mathbf{k})}{\partial x_i} - k_j \frac{\partial u_j}{\partial x_i} \frac{\partial N(\mathbf{k})}{\partial k_i} = \frac{Q(\mathbf{k})}{\omega} \quad (1)$$

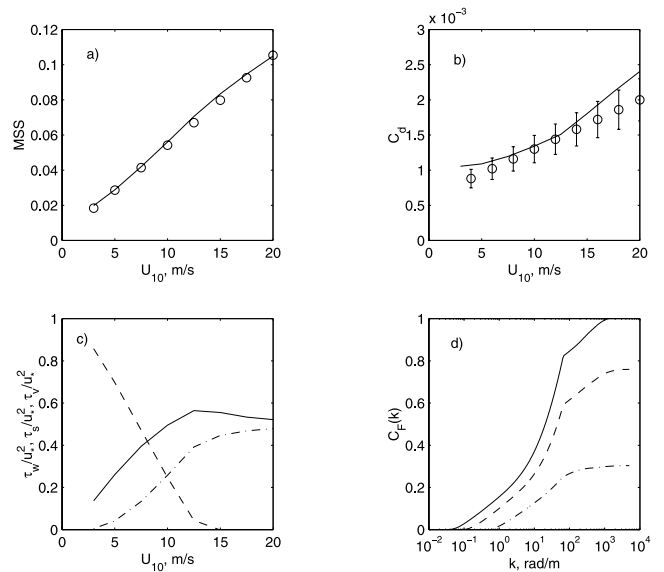


**Figure 1.** (a) Mean square slope (mss) versus wind speed. Solid line: model calculations; open circles: *Cox and Munk's* [1954] observations. (b) Sea surface drag coefficient versus wind speed. Solid line: model calculations; open circles: regression from the work of *Yelland and Taylor* [1996] with 15% error bar. (c) Stress contributions. Dashed-dotted line: stress due to separation  $\tau_s/u^2$ ; solid line: wave-induced stress  $\tau_w/u^2$ ; dashed line: viscous stress  $\tau_v/u^2$ . (d) Omnidirectional cumulative spectrum of form drag defined by (18). Dashed-dotted line: wind speed  $U_{10} = 5$  m s $^{-1}$ , spectral peak wave number  $k_p = 0.27$  rad m $^{-1}$ ; dashed line:  $U_{10} = 10$  m s $^{-1}$ ,  $k_p = 0.068$  rad m $^{-1}$ ; solid line:  $U_{10} = 15$  m s $^{-1}$ ,  $k_p = 0.030$  rad m $^{-1}$ . Results shown are for a fully developed sea  $U_{10}/C = 0.83$ .

where  $c_{gi}$  and  $u_i$  are components of the wave group velocity and the surface current respectively;  $i$  and  $j = 1, 2$ ;  $\omega$  and  $\mathbf{k}$  are the angular frequency and the wave number vector ( $k = |\mathbf{k}|$  is the wave number modulus and  $k_i$  are its components) linked by the dispersion relation:

$$\omega^2 = gk + \gamma k^3, \quad (2)$$

$g$  is the acceleration of gravity,  $\gamma$  is the surface tension,  $Q(\mathbf{k})$  is the source of wave energy. The elevation spectrum  $F(\mathbf{k})$ , the energy spectrum  $E(\mathbf{k})$ , and the wave action spectrum  $N(\mathbf{k})$  are related to each other by  $E(\mathbf{k}) = (\omega^2/k)F(\mathbf{k})$ ,  $N(\mathbf{k}) = E(\mathbf{k})/\omega = (\omega/k)F(\mathbf{k})$ . The degree of the saturation spectrum  $B(\mathbf{k})$  (the surface curvature spectrum) used throughout the paper is defined as  $B(\mathbf{k}) = k^4 F(\mathbf{k})$ . Equation (1) describes the background spectrum and its modulation. The form of the background spectrum results from a solution of equation  $Q(\mathbf{k}) = 0$ , and the modulation of the SWs by a LW can be found as a solution of the linearized equation (1) for a small disturbance of the spectrum.

[7] In the present study a model of the SW spectrum developed by *Kudryavtsev et al.* [1999] is used. In the equilibrium interval of the spectrum defined in the range  $k \gg k_p$ , where  $k_p$  is the wave number at the spectral peak, the form of the spectrum is found as a solution of the energy balance equation (1), where the energy source  $Q(\mathbf{k})$  is

$$Q(\mathbf{k}) = \omega^3 k^{-5} \left[ \beta_\nu(\mathbf{k}) B(\mathbf{k}) - B(\mathbf{k}) \left( \frac{B(\mathbf{k})}{\alpha} \right)^n + I_{pc}(\mathbf{k}/k_\gamma) \right]. \quad (3)$$

Here  $\beta_\nu(\mathbf{k}) = \beta(\mathbf{k}) - 4\nu k^2/\omega$  is the effective growth rate, which is the difference between the wind growth rate parameter  $\beta(\mathbf{k})$  and the rate of viscous dissipation ( $\nu$  is the viscosity), and  $k_\gamma = (g/\gamma)^{1/2}$  is the wave number at the minimum phase velocity. The growth rate  $\beta$  is parameterized as

$$\beta(k, \varphi) = C_\beta \left( \frac{u_*}{c} \right)^2 \cos \varphi |\cos \varphi|, \quad (4)$$

where  $u_*$  is the friction velocity,  $C_\beta$  is the growth rate coefficient, and  $\varphi$  is the angle between the wind direction and the wave component.

[8] The second term in (3) describes the nonlinear energy loss, which is associated with wave breaking at  $k < k_{wb} \approx 2\pi/0.15 \text{ rad m}^{-1}$ , generation of parasitic capillaries at  $k_{wb} < k < 1/2k_\gamma$ , and with three-wave interactions redistributing energy from a vicinity of  $k \sim k_\gamma$  toward shorter and longer waves at larger  $k$ . The third term in (3)  $I_{pc}(\mathbf{k}/k_\gamma)$  describes the cascade of energy transfer from the short gravity interval to the capillary interval due to generation of parasitic capillaries. The wave number vectors of parasitic capillaries  $k$  and the generating gravity wave  $k_g$  are collinear and their modulus is linked by

$$k_g = \frac{k_\gamma^2}{k}. \quad (5)$$

In the work of *Kudryavtsev et al.* [1999] it was argued that generation of parasitic capillaries provides the energy loss  $D(\mathbf{k}_g)$  for short gravity waves in the range of wavelength from 15 cm to  $4\pi/k_\gamma$ . The crest of longer gravity waves breaks and generates turbulence rather than generates trains of parasitic capillaries. The dimensionless source of parasitic capillaries in (3) is

$$I_{pc}(\mathbf{k}/k_\gamma) = \widehat{D}(\mathbf{k}_g) \phi(k_\gamma/k) = B(\mathbf{k}_g) \left( \frac{B(\mathbf{k}_g)}{\alpha(\mathbf{k}_g)} \right)^{n(\mathbf{k}_g)} \phi(k_\gamma/k), \quad (6)$$

where  $\widehat{D}(\mathbf{k}_g)$  is the dimensionless dissipation of short gravity waves:  $\widehat{D}(\mathbf{k}_g) \equiv \omega_g^{-3} k_g^5 D(\mathbf{k}_g)$ ,  $\omega_g = \omega(k_g)$ . Note that if the short gravity waves generating parasitic capillaries are balanced by the energy input from the wind, then  $\widehat{D}(\mathbf{k}_g)$  in (6) is equal to  $\widehat{D}(\mathbf{k}_g) = \beta_\nu(\mathbf{k}_g) B(\mathbf{k}_g)$ . The function  $\phi(k_\gamma/k)$  in (6) is a filter function, which restricts the action of the source of parasitic capillaries in  $k$ -space. Its physical meaning is that the parasitic capillaries can be generated only by short gravity waves with the wave number  $k > k_{wb} \approx 2\pi/0.15 \text{ rad m}^{-1}$ . The crest of longer gravity waves breaks and generates turbulence. Thus, the filter function has to be close to 1 in the interval  $2k_\gamma < k^2/k_{wb}$  and vanishes outside. Parameters  $n$  and  $\alpha$  in (3) are functions of the dimensionless wave number  $k_\gamma/k$ :  $1/n = (1 - 1/n_g) f(k/k_\gamma) - 1/n_g$  and  $\ln \alpha = \ln a - (1/n) \ln \widehat{C}_\beta$ , where  $\widehat{C}_\beta$  is the growth rate parameter at  $k = k_\gamma/2$ , the function  $f(k/k_\gamma)$  is equal to 1 at  $k/k_\gamma \geq 1$ , and equal to zero at  $k/k_{wb} < 1$ . A discussion on how to determine the function  $f(k/k_\gamma)$  and constants  $n_g$  and  $a$  can be found in the work of *Kudryavtsev et al.* [1999, 2002]. Constant  $a$  was determined as  $a = 2.5 \times 10^{-3}$  so that the model mean square

slope should correspond to *Cox and Munk* [1954] observations, and parameter  $n_g$  was specified as  $n_g = 5$ . Note that in the study by *Kudryavtsev et al.* [1999] constant  $n_g$  was chosen as  $n_g = 2$ . However, the value  $n_g = 5$  gives better agreement with observation in terms of the wind exponent of the interval of short gravity waves [see *Kudryavtsev et al.*, 2002] study for more details.

[9] The solution of equation  $Q(\mathbf{k}) = 0$  with the source (3) gives the shape of the equilibrium spectrum in the range from very short capillary waves to gravity waves

$$B(\mathbf{k}) = \alpha \left[ \frac{1}{2} \left( \beta_\nu(\mathbf{k}) + \left( \beta_\nu^2(\mathbf{k}) + \frac{4I_{pc}(\mathbf{k})}{\alpha} \right)^{1/2} \right) \right]^{1/n}. \quad (7)$$

The derivation of the spectrum (7) from the source (3) is given by *Kudryavtsev et al.* [1999]. Correspondence of the shape of the spectrum (7) to the measured spectra was discussed ibidem.

## 2.2. Drag of the Sea Surface

[10] Equation (7) describes statistical properties of the sea surface in terms of the wave spectrum. The wind growth rate is defined by the friction velocity  $u_*$ , which is one of the governing parameters of the wave spectrum. Thus to complete the coupled model one has to define the sea surface drag (stress). The sea surface stress  $\tau$  is supported by the viscous stress  $\tau_\nu$  and the form drag. The latter is a sum of the wave-induced stress  $\tau_w$  due to the nonseparated sheltering wind growth mechanism and the stress due to the airflow separation from breaking wave crests  $\tau_s$  [*Kudryavtsev and Makin*, 2001] so that

$$\tau \equiv u_*^2 = \tau_\nu + \tau_w + \tau_s. \quad (8)$$

The viscous stress  $\tau_\nu$  is estimated from patching the linear wind profile at the top of the molecular sublayer with the logarithmic wind profile above it

$$\tau_\nu = \frac{u_*^2}{\kappa d_\nu} \ln \frac{d_\nu \nu}{u_* z_0}, \quad (9)$$

where  $\kappa = 0.4$  is the von Karman constant,  $d_\nu = 12$  is a constant defining the height of the molecular sublayer,  $z_0$  is the roughness scale. The wave-induced stress  $\tau_w$  was defined in terms of the growth rate  $\beta$  as

$$\tau_w = \frac{\rho_w}{\rho_a} \int \int \beta c^2 B(\mathbf{k}) \cos \varphi d \ln k d \varphi, \quad (10)$$

where  $\rho_a$  and  $\rho_w$  are density of air and water,  $c = \omega/k$  is the phase speed, and the growth rate coefficient  $C_\beta$  in  $\beta$  (4) was defined as  $C_\beta = c_\beta (\rho_a/\rho_w) / \kappa (\ln(\pi/kz_0) - \kappa c/u_*)$  [*Stewart*, 1974] at  $c_\beta = 2$ . The separation stress  $\tau_s$  was obtained following the analogy between the airflow separation from a backward facing step and the breaking wave

$$\tau_s = \varepsilon_b \gamma \int u_s^2 \cos \varphi k^{-1} \Lambda(\mathbf{c}) d\mathbf{c}, \quad (11)$$

where  $\varepsilon_b = 0.5$  is the steepness of a breaking wave,  $\gamma \sim 1$  is a constant,  $u_s = u_*/\kappa \ln(1/kz_0) \cos \varphi - c$  is the reference

wind speed, and  $\Lambda(\mathbf{c})d\mathbf{c}$  is the total length of wave breaking fronts per unit surface travelling with velocities from  $\mathbf{c}$  to  $\mathbf{c} + d\mathbf{c}$  as introduced by *Phillips* [1985] for the spectral description of wave breaking statistics. To express  $\Lambda(\mathbf{c})$  through the wave spectrum we note that the same wave breaking statistics defines the energy loss due to wave breaking [*Phillips*, 1985]

$$dD(\mathbf{c}) = bg^{-1}c^5\Lambda(\mathbf{c})d\mathbf{c}, \quad (12)$$

where  $dD(\mathbf{c})$  is the energy loss by the breaking front and  $b$  is an empirical constant. In the present SWs model the energy dissipation due to wave breaking is parameterized as a  $(n + 1)$  power of the saturation spectrum (second term in (7)). In terms of  $dD(\mathbf{c})$  this parameterization coincides with (12) if function  $\Lambda(\mathbf{c})$  is defined as

$$\Lambda(\mathbf{c}) = \frac{g}{c^4} \left( \frac{B(\mathbf{k})}{\alpha} \right)^{n+1} \quad (13)$$

with  $b = 2\alpha$ . In the gravity range  $\alpha = 5 \times 10^{-3}$ . It was shown that the main contribution to  $\tau_s$  comes from the short gravity wind waves due to their high surface density.

[11] The resistance law defining the aerodynamical roughness of the sea surface follows from equations (8) to (11) and reads

$$\frac{1}{\kappa d_v} \ln \frac{d_v \nu}{u_* z_0} + \int_{\varphi} \int_k \Upsilon_w(\mathbf{k}) d\varphi d \ln k + \int_{\varphi} \int_{k < k_{wb}} \Upsilon_s(\mathbf{k}) d\varphi d \ln k = 1, \quad (14)$$

where  $\Upsilon_w(\mathbf{k})$  and  $\Upsilon_s(\mathbf{k})$  are spectra of the wave-induced and the separation stress normalized on  $u_*^2$

$$\Upsilon_w(\mathbf{k}) = c_{\beta} \kappa^{-1} \left( \frac{\rho_w}{\rho_a} \right)^2 \left( \ln \frac{\pi}{k z_0} - \frac{ck}{u_*} \right) \cos^3 \varphi B(\mathbf{k}), \quad (15)$$

$$\Upsilon_s(\mathbf{k}) = \frac{\varepsilon_b \gamma}{2\kappa} \left( \ln \frac{1}{k z_0} \cos \varphi - \frac{ck}{u_*} \right)^2 \cos \varphi \left( \frac{B(\mathbf{k})}{\alpha} \right)^{n+1}. \quad (16)$$

The resistance law explicitly relates the wave saturation spectrum to the roughness scale  $z_0$  of the sea surface. The spectrum (7) and the resistance law (14) constitute a coupled self-consistent system. The SW spectrum (7) depends on the friction velocity via the growth rate. Relating the friction velocity to the wind speed at the reference level (here taken at 10 m)

$$u_* = C_d^{\frac{1}{2}} U_{10} \equiv \frac{\kappa}{\ln(10/z_0)} U_{10}, \quad (17)$$

the SW spectrum is related to the surface roughness scale, whereas  $z_0$  is dependent on the wave spectrum via (14).

[12] In Figures 1a and 1b the background wind dependence of two general elements of the coupled model: the mean square slope (calculated through the spectrum (7)) and the drag coefficient (calculated through (17) and  $z_0$  obtained from the resistance law (14)) is shown for a fully developed sea. The model mean square slope closely coincides with the *Cox and Munk* [1954] observations, while the model drag coefficient is in agreement with the *Yelland and Taylor*

[1996] data within their 15% confidence interval. At low winds the surface drag is supported mainly by the viscous stress, while at moderate and strong winds the form drag dominates. This is illustrated by Figure 1c, where the stresses  $\tau_w/u_*^2$ ,  $\tau_w/u_*^2$ , and  $\tau_s/u_*^2$  (normalized on the total stress so that their sum equals 1) are shown as a function of the wind speed. Figure 1d demonstrates the cumulative spectrum of the form drag

$$C_F(k) = \int_0^k d \ln k \left( \int_{\varphi} (\Upsilon_w + \Upsilon_s) d\varphi \right) \quad (18)$$

at various wind speeds. SWs with the wave number  $k > 10 k_p$  support almost 100% of the form drag. Hence, it can be anticipated that the SW modulation can effectively affect the turbulent airflow over the dominant surface waves. Since the contribution of the form drag to the total stress increases with an increase of the wind speed, the impact of SWs on the turbulent airflow becomes also stronger.

### 3. SWs and the Airflow Over a LW

[13] A LW modulates the SWs and perturbs the turbulent airflow. Since the airflow and the SWs are coupled a feedback between the LW-induced variation in the turbulent airflow and the SW modulation should exist. Below we consider the modulation in each of the elements of the coupled airflow–SW system and show how they are coupled.

[14] Assume that a LW with the amplitude  $A$ , frequency  $\Omega$  and wave number  $K$  satisfying the condition  $KA \ll 1$  is travelling in the  $x_1$ -direction, and the sea surface displacement of the LW is

$$\zeta(\mathbf{x}, t) = \frac{1}{2} (A e^{i(kx_1 - \Omega t)} + c.c.). \quad (19)$$

The LW causes a small perturbation in all characteristics of the sea surface and the airflow. If  $Y$  is any parameter like the wave action spectrum or the friction velocity, then its wave-induced variation  $\tilde{Y}$  is

$$\tilde{Y}(\mathbf{x}, t) = \frac{1}{2} (\hat{Y} e^{i(kx_1 - \Omega t)} + c.c.). \quad (20)$$

where  $\hat{Y}$  is a complex amplitude. A negative imaginary part of  $\hat{Y}$  means that the maximum of the  $Y$ -variation is shifted to the forward slope of the LW. Throughout the paper the description of the LW-induced variation of any quantity  $Y$  will be done in terms of the MTF  $M_Y$  defined as

$$M_Y = \frac{\hat{Y}}{AK\bar{Y}}, \quad (21)$$

where  $\bar{Y}$  is the mean value of  $Y$ .

#### 3.1. Modulation of the SW Spectrum

[15] The modulation of a SW by the LW is described as a solution of the perturbed energy balance equation (1). When the wave number  $k$  of the modulating SW is much larger than  $K$  the SW group velocity is much smaller than the LW

phase velocity, and the linearized wave action conservation equation (1) for a small disturbance  $\tilde{N}$  (i.e.,  $\tilde{N}/\bar{N} \ll 1$ ) is reduced to [e.g., *Alpers and Hasselmann, 1978*]

$$\frac{\partial \tilde{N}}{\partial t} - k_1 \frac{\partial u}{\partial x_1} \frac{\partial \bar{N}}{\partial k_1} = \frac{\tilde{Q}}{\omega}, \quad (22)$$

where  $\tilde{Q}$  is the variation of the energy source. In the present model  $\tilde{Q}$  is to be found as a small perturbation of the energy source (3). As follows from (3), the disturbance in  $Q$  can be caused by the surface wind stress variation via the growth rate parameter  $\beta$  which enters the energy wind input described by the first term in (3), by the variation in the SW spectral density (which enters the wind input and the nonlinear energy losses described by the first and second terms in (3), respectively, and by the variation in the parasitic capillaries energy source represented by (6) (the third term in (3)). An expression for the small disturbance of the energy source  $Q$  can be easily found by a linear decomposition of each of its components. After some reorganization the linearized expression for the small variation of the energy source  $Q$  reads

$$\frac{\tilde{Q}}{\omega} \frac{1}{\omega \bar{N}} = \tilde{\beta} - (n\beta_\nu + (n+1)\beta_{pc}) \frac{\tilde{B}(\mathbf{k})}{\bar{B}(\mathbf{k})} + \beta_{pc}(n(\mathbf{k}_g) + 1) \frac{\tilde{B}(\mathbf{k}_g)}{\bar{B}(\mathbf{k}_g)}, \quad (23)$$

where  $\beta_{pc} = I_{pc}(\mathbf{k})/B(\mathbf{k})$  is the growth rate parameter of parasitic capillaries.

[16] Equations (22) and (23) can be solved to obtain the amplitude of the SW spectrum variation. In terms of the MTF (21) this solution is

$$M(\mathbf{k}) = - \left( \frac{1 - i\tau_r}{1 + \tau_r^2} \right) \frac{k_1}{\bar{N}(\mathbf{k})} \frac{\partial \bar{N}(\mathbf{k})}{\partial k_1} + \frac{\tau_r + i}{1 + \tau_r^2} \cdot [2\tau_* M_* + \tau_{pc}(n(\mathbf{k}_g) + 1)M(\mathbf{k}_g)], \quad (24)$$

where  $M(\mathbf{k}) = \hat{N}(\mathbf{k})/(KAN\bar{N}(\mathbf{k}))$ ;  $\tau_r = (T_r\Omega)^{-1}$  is the dimensionless relaxation parameter of the spectrum;  $T_r$  is the relaxation time defined as

$$T_r^{-1} = \omega(n\beta_\nu + (n+1)\beta_{pc}), \quad (25)$$

$\tau_* = (\omega\beta/\Omega)$  is the dimensionless growth rate parameter;  $\tau_{pc} = (\omega\beta_{pc}/\Omega)$  is the dimensionless growth rate parameter of the parasitic capillaries;  $M_* = \hat{u}_*/(KA\bar{u}_*)$  is the MTF of the friction velocity. As the surface stress  $\tau = u_*^2$ , the MTF of the stress is  $M_\tau = 2 M_*$ . Equation (24) describes the SW modulation caused by interaction of the SW with the LW orbital velocity (first term), the modulation of the wind surface stress (second term), and the modulation of the short gravity wave emitting parasitic capillaries represented by the third term with  $M(\mathbf{k}_g)$  being the MTF of this gravity wave. The strain factor in (24) can be rewritten as

$$\frac{k_1}{N(k, \varphi)} \frac{\partial N(k, \varphi)}{\partial k_1} = \cos^2 \varphi \frac{\partial \ln N}{\partial \ln k} - \sin \varphi \cos \varphi \frac{\partial \ln N}{\partial \varphi}. \quad (26)$$

[17] Equation (24) predicts the following asymptotic regimes of the SW modulation. If the relaxation time for a given spectral component is much larger than the period of

the LW, i.e.,  $\tau_r \ll 1$ , then only the first term remains on the right-hand side of equation (24), which means that the SW interacts with the LW adiabatically. It experiences straining with an increase of the modulation on the LW crest:  $M \simeq m_k$ , where  $m_k$  is the wave number exponent of the wave action spectrum [*Phillips, 1977*]. If the LW travels in the crosswind direction then the SW modulation vanishes. At high wind speeds for short gravity and capillary gravity waves the relaxation time is much smaller than the period of the LW, i.e.,  $\tau_r \gg 1$ . In this case the SW modulation due to the straining represented by the first term on the right-hand side of (24) is negligible, and the modulation of the wind surface stress is the only source of the modulation of these waves. The SW modulation is completely defined by the magnitude of the local stress variation, which results from the dynamics of the airflow over the LW

$$M(\mathbf{k}) \simeq \frac{2}{n} M_*. \quad (27)$$

In the capillary gravity range parameter  $n = 1$ , hence the MTF of the SW is twice the MTF of the surface stress. Well inside the capillary range the mechanism of generation of parasitic capillaries represented by the third term on the right-hand side of (24) is dominant. One can anticipate that the condition  $\tau_r \gg 1$  is fulfilled here at any wind speed and any parameters of the LW, hence  $M(\mathbf{k}) \simeq (\tau_{pc}/\tau)(n(\mathbf{k}_g) + 1)M(\mathbf{k}_g)$ . At low and moderate wind speed the energy loss is due to viscous dissipation, and therefore  $\beta_{pc} \simeq -\beta_\nu$  (the latter is  $\beta_\nu = -4\nu k^2/\omega$ ) and  $T_r^{-1} \simeq -\omega\beta_\nu$ . The ratio  $(\tau_{pc}/\tau) \simeq 1$  and thus the magnitude of the MTF in the capillary range is amplified  $(n(\mathbf{k}_g) + 1)$ -times compared to the MTF of the short gravity wave, i.e.,

$$M(\mathbf{k}) = (n(\mathbf{k}_g) + 1)M(\mathbf{k}_g). \quad (28)$$

At high wind speed the rate of generation of parasitic capillaries is balanced by the nonlinear quadratic energy loss. Hence, the relaxation time is  $T_r^{-1} \simeq \omega(n+1)\beta_{pc} = 2\omega\beta_{pc}$ , and, as follows from (24), the MTF in the capillary range is

$$M(\mathbf{k}) = \frac{1}{2}(n(\mathbf{k}_g) + 1)M(\mathbf{k}_g), \quad (29)$$

i.e., at high wind speed the amplification factor reduces by a factor of two as compared to (28).

[18] To resolve equation (24), the LW-induced variation of the wind surface stress or the friction velocity should be known. This is obtained from a model of the turbulent airflow over waves by *Kudryavtsev et al.* [2001a] supplied with the resistance law relating the SW modulation to the varying surface roughness.

### 3.2. Impact of the SW Modulation on the Surface Roughness

[19] According to (14) it is anticipated that the SW modulation could cause the variation of the aerodynamic roughness along the LW profile. How can we estimate this variation? The turbulent airflow over the LW can be divided into two regions, the outer (OR) and the inner (IR) region [*Belcher and Hunt, 1993*]. In the OR the wave-induced

motion experiences inviscid undulation, while in the IR the motion is strongly affected by the turbulence shear stress. A scale  $l$  of the IR is defined by *Belcher and Hunt* [1993] as

$$Kl = \frac{2\kappa u_*}{|\bar{u}_1(l) - C|}, \quad (30)$$

where  $C$  is the LW phase velocity, and  $\bar{u}_1(l)$  is the mean wind velocity described by the logarithmic profile at  $z = l$ . Well inside the IR at  $z \ll l$  the perturbed wind velocity profile can be locally approximated by the logarithmic shape. It means that expression (14) can be considered as a local resistance law if the scale of the modulated wave is much smaller than the IR scale, i.e.,  $k^{-1} \ll l$ . The range of SWs modulated by the LW can be defined as  $k > 10 K$ . Hence, for the longest modulated SW the condition  $k^{-1} \ll l$  is equivalent to  $10 Kl \gg 1$ . Since a rough estimate of (30) is  $Kl = 0.1$  or less [*Kudryavtsev et al.*, 2001a] the above condition is not fulfilled for all modulated waves. However, the main contribution to the wave-induced stress and the airflow separation stress comes from the shortest waves (Figure 1d), which are located well inside the IR. Hence, equation (14) can be considered as the local resistance law, which is valid at any phase of the LW.

[20] The resistance law for a small perturbation in the roughness scale  $\tilde{z}_0$  and the spectrum  $\tilde{B}$  can be written as

$$-\frac{1}{\kappa d_v} \frac{\tilde{z}_0}{z_0} + \frac{\tilde{z}_0}{z_0} \int_{\varphi} \int_{k>km} z_0 \Upsilon'_{z_0}(\mathbf{k}) d\varphi d \ln k + \int_{\varphi} \int_{k>km} \Upsilon'_B(\mathbf{k}) \tilde{B} d\varphi d \ln k = 0, \quad (31)$$

where  $\Upsilon = \Upsilon_w + \Upsilon_s$  is the spectrum of the form drag,  $\Upsilon'_{z_0}$  is its partial derivative with respect to the roughness scale,  $\Upsilon'_B$  is the partial derivative with respect to the saturation spectrum, and  $k_m = 10 K$  is the lower limit of the range of the modulated waves. In terms of the MTF the last equation reads

$$M_{z_0} = \frac{\int_{\varphi} \int_{k>km} \tilde{B}(\mathbf{k}) \Upsilon'_B(\mathbf{k}) M_B(\mathbf{k}) d\varphi d \ln k}{(\kappa d_v)^{-1} - \int_{\varphi} \int_{k>km} z_0 \Upsilon'_{z_0}(\mathbf{k}) d\varphi d \ln k} \quad (32)$$

[21] To derive equations (31) and (32) from the background resistance law (14) we have neglected terms containing the variation of  $u_*$  with respect to the LW disturbances. It can be shown that the ratio of these omitted terms to the retained one is of the order  $1/\ln(l/\tilde{z}_0) \sim 0.1$ .

[22] Equation (32) relates the amplitude of the roughness scale variation along the LW to the modulation of the SW spectrum. Since the spectrum of the airflow separation stress (16) is proportional to  $B^{n_s+1}$  while the spectrum of the wave-induced stress (15) is proportional to  $B$ , one can anticipate that the modulation of wave breaking is mainly responsible for the modulation of the roughness scale.

### 3.3. Surface Stress

[23] The surface stress or the friction velocity MTF  $M_*$  is defined by using a simplified model of the airflow over surface waves by *Kudryavtsev et al.* [2001a]. Significant simplification was achieved by division of the airflow over the wave into two regions, the outer (OR) and the inner (IR) region [*Belcher and Hunt*, 1993]. The scale of the IR is

defined by (30). In the OR at  $z > l$  the Reynolds stresses are decorrelated with the wave, hence the wave-induced motion can be treated as inviscid wave-induced undulation. The wave-induced variation of vertical and horizontal velocity results from the approximate solution of the Rayleigh and vorticity conservation equations. The profile for the vertical and horizontal velocity is

$$\frac{\hat{w}(z)}{AK} = i(\bar{u}_1(z) - C)e^{-Kz}, \quad (33)$$

$$\frac{\hat{u}_1(z)}{AK} = (\bar{u}_1(z) - C)e^{-Kz} + \frac{2u_*}{\kappa} \cos\varphi \int_{Kz}^{\infty} e^{-kz'} d \ln Kz' \quad (34)$$

where  $z = x_3 - \zeta(x, t)$  is the vertical coordinate in the wave following coordinate system.

[24] In the IR, the wave-induced Reynolds stress significantly affects the airflow dynamics. A description of the IR dynamics by *Kudryavtsev et al.* [2001a] is based on the vorticity conservation equation written in terms of the shear stress variation (see their equation (49)). To derive an explicit relation for the LW-induced surface stress variation and to show the effect of varying surface aerodynamic roughness on the surface stresses and thus on the SW modulations the problem could be simplified further by approximating the profile of the wind velocity undulation inside the IR (at  $z < l$ ) by the logarithmic shape, i.e.,

$$u_1(x, t, z) = u_s(x, t) + c_u \ln \frac{z}{z_0(x, t)}, \quad (35)$$

where  $u_s$  is the LW orbital velocity and constant  $c_u$  is chosen so as to patch the wind velocity profile described by (34) at  $z = l$ :  $c_u = \Delta u_1 / \ln(l/z_0(x, t))$ , where  $\Delta u_1 = u_1(x, t, l) - u_s(x, t)$  is the wind velocity difference over the IR. The linearized equation (35) gives the following profile for the amplitude of the wave-induced variation of the wind velocity

$$\hat{u}_1(z) = \left( \hat{u}_s - \frac{\bar{u}_*}{\kappa} \cos\varphi \frac{\hat{z}_0}{z_0} \right) + \hat{c}_u \ln \frac{z}{z_0}, \quad (36)$$

where  $\hat{c}_u = (\Delta \hat{u}_1 + (\bar{u}_*/\kappa) \cos\varphi (\hat{z}_0/\tilde{z}_0)) \ln^{-1}(l/z_0)$  and  $\Delta \hat{u}_1 = \hat{u}_1(l) - \hat{u}_s$ .

[25] To estimate the friction velocity MTF we account for the fact that in the IR the turbulent stress  $\tau$  is in the local balance with the wind velocity shear. It follows

$$\tau = \kappa^2 z^2 \left( \left( \frac{\partial u_1}{\partial z} \right)^2 + \left( \frac{\partial u_2}{\partial z} \right)^2 \right), \quad (37)$$

where  $u_1 = \bar{u}_1 + \tilde{u}_1$  and  $u_2 = \bar{u}_2$ . Accounting for (36) the LW-induced variation of the surface stress in terms of the friction velocity MTF reads

$$M_* = \cos^2\varphi \left[ M_{\Delta u} + M_{z_0} \ln^{-1} \frac{l}{z_0} \right], \quad (38)$$

where  $M_{\Delta u} = \Delta \hat{u}_1 / (KA \bar{u}_1(l))$  is the normalized amplitude of the difference of the LW-induced wind velocity variation over the IR. Using (34)

$$M_{\Delta u} = 1 - \frac{2C}{\bar{u}_1(l)} + 2 \ln^{-1} \frac{l}{z_0} \int_{Kl}^{\infty} e^{-Kz'} d \ln Kz', \quad (39)$$

where the roughness scale MTF  $M_{z_0}$  is defined by (32). Equation (38) relates the modulation of the friction velocity to the undulation of the airflow in the OR and to the modulation of the surface roughness. The latter, in turn, depends via (32) on the wave spectrum modulation. As follows from (39), the impact of the airflow undulation on the surface stress variation depends on wave age of the LW. For a young wave (the wave age parameter  $C/\bar{u}_1(l)$  is small) the airflow undulation enhances the surface stress over the LW crest, while for an old wave ( $C/\bar{u}_1(l)$  is large) the surface stress is enhanced over the LW trough.

[26] Equations (24), (32), and (38) constitute a closed system describing the coupled dynamics of SWs and the turbulent airflow over a LW. As follows from these equations, the SW modulation depends on the surface stress variation  $M_*$ , which is determined by the airflow undulation  $M_{\Delta u}$  and the roughness scale modulation  $M_{z_0}$ . The latter, in turn, depends on the SW modulation affecting the form drag. This scheme provides a self-consistent coupling of SWs and the airflow over the LW.

#### 4. SWs and the Airflow Modulation: The Model and Measurements

[27] The modulation of wave breaking plays a key role in the coupled dynamics of SWs and the airflow over the dominant LW. The form drag is supported by the airflow separation from breaking waves and breaking waves generate parasitic capillaries. Therefore a strong modulation in wave breaking can significantly affect the surface stress modulation and thus the modulation of SWs.

##### 4.1. Modulation of Wave Breaking and the SW Spectrum

[28] A field estimate of the wave breaking modulation by LWs obtained by *Dulov et al.* [2002] is shown in Figure 2. The data correspond to the whitecap coverage variation caused by LWs with the wave number in the range from 0.1 to 0.25  $\text{rad m}^{-1}$ . Despite the large scatter (error bars correspond to the 95% confidence level) the measurements apparently show a very strong modulation of wave breaking characterized by the averaged MTF amplitude of about 22 and by the enhancement on the crests of the LW.

[29] To simulate the measurements we follow *Phillips* [1985] and relate the whitecap coverage  $q$  to the distribution

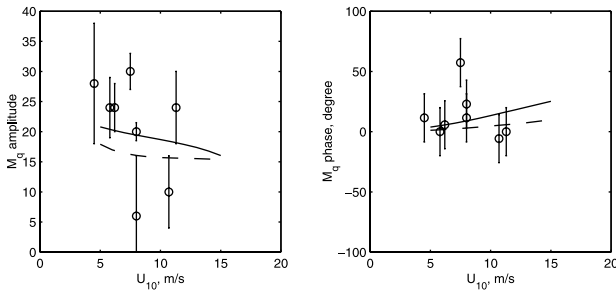


**Figure 2.** Amplitude and phase of the MTF for the whitecap coverage as a function of wind speed. Open circles: field observation by *Dulov et al.* [2002], error bars correspond to 95% confidence level. Model calculations, solid line: LW wave number is 0.1  $\text{rad m}^{-1}$ ; dashed line: LW wave number is 0.25  $\text{rad m}^{-1}$ .

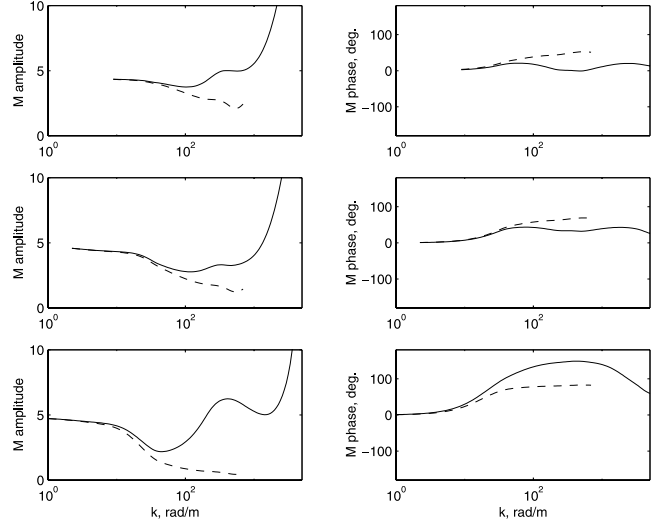


**Figure 3.** Amplitude (left column) and phase (right column) of the SW spectrum MTF for wind speed 10  $\text{m s}^{-1}$  and for different inverse LW age parameter, upper panels:  $U_{10}/C = 3$ ; middle panels:  $U_{10}/C = 1.5$ ; lower panels:  $U_{10}/C = 0.5$ . Solid line: modulation of SWs by all mechanisms; dashed line: modulation of SWs due to orbital velocities only. The LW travels in the wind direction.

function  $\Lambda$  as  $q = \int k^{-1} \Lambda(\mathbf{c}) d\mathbf{c}$ . Accounting for (13) the whitecap coverage MTF is

$$M_q = (n_g + 1) \frac{\int_{k_m}^{-k_g} d \ln k \int_{\varphi} d\varphi M(\mathbf{k}) (\bar{B}(\mathbf{k})/\alpha_g)^{n_g+1}}{\int_0^{k_g} d \ln k \int_{\varphi} d\varphi (\bar{B}(\mathbf{k})/\alpha_g)^{n_g+1}}, \quad (40)$$

where  $k_g$  is the upper limit of the range of breaking waves generating whitecaps. We assumed that the wave number of the shortest wave, which generates a whitecap, is  $k_g \approx 2\pi/0.5 \text{ rad m}^{-1}$ . Equation (40) has two remarkable features. The first feature is that the gravity waves providing the modulation of  $q$  should be modulated by the LW adiabatically due to a small relaxation parameter (for  $\tau_r \ll 1$  the first term in (24) is the leading one). It means that the airflow itself does not affect the wave breaking modulation. The second feature of (40) is that the amplitude of the whitecap coverage modulation is in  $(n_g + 1)$ -times amplified in comparison with the gravity wave MTF. The model calculations of the whitecap coverage MTF are done according to (40) and (24) and are shown in Figure 2 for a LW with the wave number 0.1  $\text{rad m}^{-1}$  and 0.25  $\text{rad m}^{-1}$ . Overall, the model results are consistent with measurements predicting a large MTF amplitude and the enhancement of wave breaking at the LW crest.

[30] The model calculations of the SW spectrum MTF for the wind speed of 10  $\text{m s}^{-1}$  and for a LW characterized by the inverse wave age parameter  $U_{10}/C = 0.5$ ,  $U_{10}/C = 1.5$  and  $U_{10}/C = 3$  travelling in the wind direction are shown in Figure 3. The model “reference” runs when the modulation of the surface stress and the modulation of the rate of parasitic capillaries generation are switched off are shown by the dashed line. In all cases the longest SWs experience behavior typical for the adiabatic modulation (the relaxation parameter  $\tau \ll 1$ ) with  $|M| = m_k \simeq 4.5$  and with an increase of the SW amplitude on the LW crest. On the other hand, the

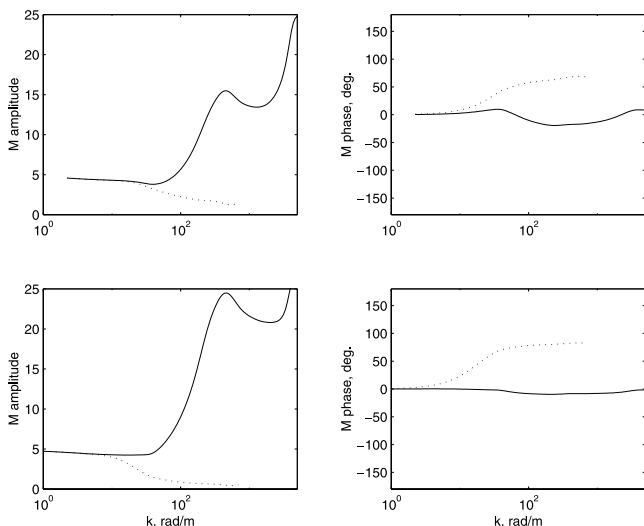


**Figure 4.** The same as in Figure 3, but the LW travels opposite to the wind direction. Upper panels:  $U_{10}/C = 1.5$ ; lower panels:  $U_{10}/C = 0.5$ .

range of shortest gravity and capillary gravity waves is significantly affected by the LW-induced variation of the surface stress, which follows from a comparison with the reference run. In this interval the reference run exhibits the SW modulation typical for the relaxation theory, which predicts suppression of the SW modulation and the shift of its phase toward the convergence of the LW orbital velocity (the MTF phase is  $\pi/2$ ) at large  $\tau$ . Accounting for the surface stress significantly increases the MTF amplitude and shifts the phase toward the region of the enhanced surface stress. This effect is clearly pronounced in the case of swell ( $U_{10}/C = 0.5$ ). A strong enhancement of the surface stress in the vicinity of the LW trough (see also Figure 5) results in the corresponding enhancement of the SW amplitude. A significant increase of the SW modulation in the capillary range is another remarkable feature of model results. This effect is related to the mechanism of generation of parasitic capillaries. The modulation of short gravity waves and their small-scale wave breaking at the wave number  $k_g$  causes the modulation in the rate of generation of parasitic capillaries at the wave number  $k$  linked to  $k_g$  by (5). As it was discussed (see equation (28)) the amplitude of the capillary wave MTF is amplified  $(n(k_g) + 1)$ -times in comparison with  $|M(k_g)|$  of the generating gravity wave. This mechanism can be referred to as the cascade mechanism of the capillary wave modulation.

[31] Figure 4 shows the SW spectrum MTF for the case when a LW travels against the wind direction. In this case the amplitude of the SW modulation is significantly enhanced. The SW modulation increases with the increase of the phase velocity of the LW. This effect is a consequence of a strong wind stress modulation, which is much stronger when the LW travels opposite to the wind direction (see Figure 5). Note that the reference runs dramatically underestimate the SW modulation.

#### 4.2. Modulation of the Sea Surface Drag

[32] Figure 5 illustrates the MTF for the roughness scale and the surface stress variation for a LW propagating in and

against the wind direction. In both cases the amplitude of the roughness scale modulation is large, and the enhancement of  $z_0$  occurs at the LW crest or on the forward face in a case of swell ( $U_{10}/C < 0.83$ ) travelling in the wind direction. For a fast LW travelling opposite the wind  $|M_{z_0}|$  attains the maximal magnitude due to the strong SW modulation. The dependence of the surface stress modulation defined by (38) as  $2M_*$  on the LW inverse wave age parameter is quite different at fair and head winds. In the former case there is a minimum of the amplitude of the stress modulation at  $U_{10}/C \approx 1$ . At smaller  $U_{10}/C$  the amplitude of  $M_\tau$  increases again but its phase shifts toward the LW trough. This effect is related to the distribution of the wind speed over the IR (equation (39)) when the inverse age parameter is increasing. For a slow LW the wind accelerates over the LW crest, while for a fast LW over its trough. At head winds the amplitude of the stress modulation is much higher than at fair winds and monotonically decreases with an increase of inverse wave age. The phase of the stress MTF is about  $0^\circ$  that means that the enhancement of the surface stress occurs over the LW crest. As it was mentioned above the behavior of very short gravity and capillary-gravity waves along the LW is completely defined by the surface stress modulation. The high amplitude of the SW modulation at head winds (Figure 4) results from a strong stress modulation.

[33] The surface stress significantly affects the SW modulation, while the role of wave breaking in the stress modulation could be significant. Figure 6 illustrates the relative contribution of the roughness scale modulation to the total stress modulation and the relative contribution of the wave breaking modulation to the roughness scale modulation at fair and head winds of 5 and 10  $\text{m s}^{-1}$ . At fair wind of 10  $\text{m s}^{-1}$  the roughness scale modulation, which is provided by the wave-induced momentum flux  $\tau_w$  and by the airflow separation from breaking waves  $\tau_s$ , plays the dominant role in the surface stress variation along the LW with the inverse wave age parameter  $U_{10}/C > 1$ . At low

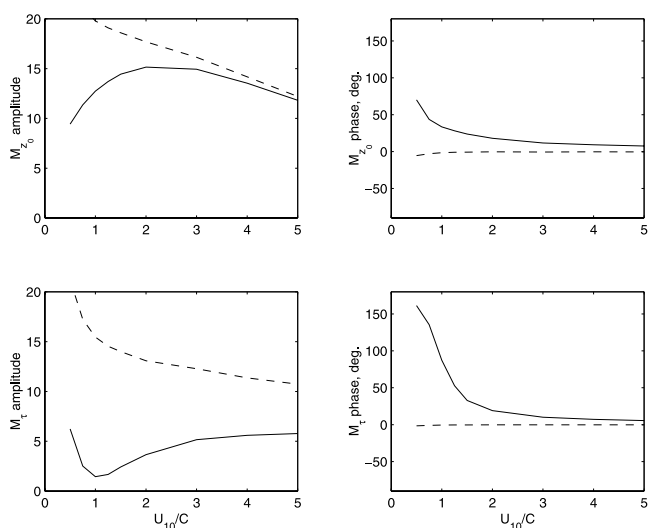


**Figure 5.** Amplitude and phase of the MTF for the surface roughness scale, upper panels, and of the MTF for the surface wind stress, lower panels versus  $U_{10}/C$  for wind speed 10  $\text{m s}^{-1}$ . Solid line: LW travels in the wind direction; dashed line: LW travels opposite to the wind direction.

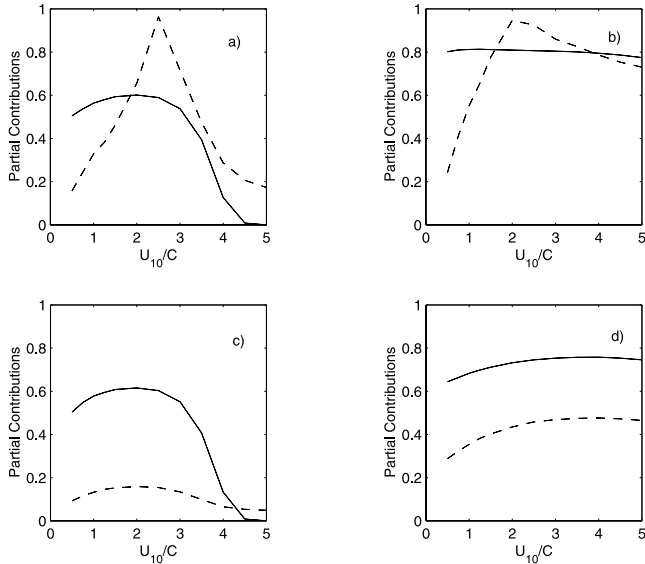


**Figure 6.** Relative contribution of the roughness scale modulation to the total stress modulation (dashed lines) and relative contribution of the wave breaking modulation to the roughness scale modulation (solid lines). (a) LW travels in the wind direction; the wind speed is  $5 \text{ m s}^{-1}$ . (b) LW travels in the wind direction; the wind speed is  $10 \text{ m s}^{-1}$ . (c) LW travels opposite to the wind direction; the wind speed is  $5 \text{ m s}^{-1}$ . (d) LW travels opposite to the wind direction; the wind speed is  $10 \text{ m s}^{-1}$ .

fair winds the roughness modulation dominates the surface stress modulation only if inverse age of a LW is in the vicinity of  $U_{10}/C \approx 2.5$ . As follows from equations (38) and (39) in this range of  $U_{10}/C$  the LW-induced wind velocity variation over the IR is small, and the surface roughness modulation is the only source of the surface stress modulation. At head wind of  $10 \text{ m s}^{-1}$ , the contribution of the  $z_0$  modulation to the surface stress is about twice less than at fair winds, and at low head winds its impact becomes negligible. At high wind speed the wave breaking modulation provides the dominant part of the aerodynamical roughness scale modulations (about 80%). The airflow separation from breaking waves provides about 50% of the wave-induced stress ( $\tau_s/\tau_w \approx 0.5$  at  $10 \text{ m s}^{-1}$ ) (see Figure 1c), but strong modulation of wave breaking by LW results in its dominant role in the roughness scale modulation. At low winds and inverse age of a LW of  $U_{10}/C < 3$  the wave breaking modulation also significantly affects the roughness scale modulation. However, its impact vanishes at larger inverse age. This effect is due to narrowing of the spectral interval of modulated breaking waves with increasing inverse age. By other words the contribution of wave breaking events correlated with the LW decreases with increasing of inverse age of a LW.

[34] Thus wave breaking plays a dominant role in the roughness scale and surface stress modulation at moderate and high wind speeds. At low winds the wave breaking also significantly affects the roughness scale modulation, but under these conditions the surface stress modulation is mainly determined by the wind velocity undulation over the LW and not by the roughness scale modulation.

### 4.3. Comparison with Measurements

[35] *Miller and Shemdin* [1991] studied the modulation of wind SWs by a mechanically generated LW with a period of 2 s in a wave tank for different wind speeds. The SW modulation was obtained from measurements of the surface slope using a laser-optical slope sensor at fetch of 24 m. The observations were transformed from frequency to wave number space taking into account the Doppler shift due to the LW orbital velocities. The frequency of the observed SWs ranged from 14 to 30 Hz ( $k \approx 300\text{--}700 \text{ rad m}^{-1}$ ). For given wind speed, the observed modulation amplitudes and phase show little dependence on the SW wave number. Therefore we averaged the results for the different wave numbers and compared them to the modulation calculated for a SW with  $k = 500 \text{ rad m}^{-1}$ . The 10 m wind speed  $U_{10}$  is calculated from the reported wind speeds in the middle of the tank and an estimate of the drag.

[36] The amplitude and the phase of the SW spectrum MTF are shown in Figure 7. According to measurements the amplitude of the SW modulation increases with an increase of the wind speed, and the area with enhanced SW energy shifts from the LW forward face toward its crest. The model reproduces the measurements reasonably well apart from some underestimation of the phase. However, the model reproduces correctly the tendency of increasing the amplitude and decreasing the phase with increasing the wind speed. The reference runs accounting for the straining factor only are failed to reproduce the measurements. The main mechanism responsible for the high SW modulation is the modulation in the surface stress plotted in Figure 7. At given LW frequency the amplitude of the surface stress increases with the wind increasing attaining the magnitude

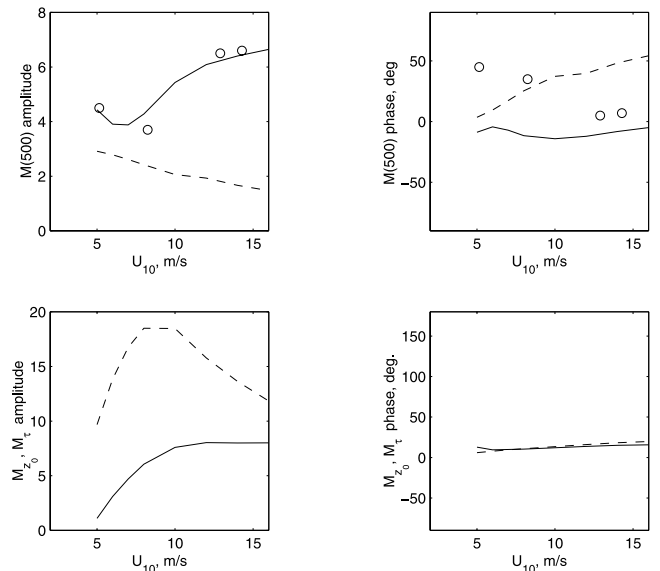


**Figure 7.** Amplitude and phase of the SW spectrum MTF in a wave tank experiment [*Miller and Shemdin*, 1991] compared with calculations, upper panels. Open circles: measurements; solid line: modulation of SWs by all mechanisms; dashed line: modulation of SWs due to orbital velocities only. Amplitude and phase of the MTF for the roughness scale (dashed line) and the surface stress (solid lines), lower panels.

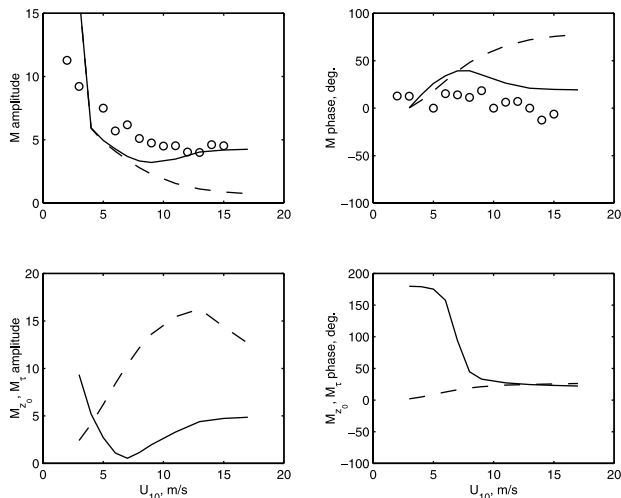


**Figure 8.** Amplitude and phase of the hydrodynamic MTF as a function of wind speed. Open circles: data compiled from the work of *Hara and Plant* [1994]; solid line: modulation of SWs by all mechanisms; dashed line: modulation of SWs due to orbital velocities only, upper panel. Amplitude and phase of the MTF for the roughness scale (dashed line) and the surface stress (solid lines), lower panels. The LW frequency is 0.25 Hz.

$M_\tau = 2|M_*| \simeq 7$ . In the capillary gravity range of the spectrum the wind exponent is about 2 and, as it follows from (27), the SW spectrum MTF at high winds follows the surface stress MTF. This effect is apparently illustrated by Figure 7. To show the aerodynamical characteristics of the LW surface the roughness scale MTF is also plotted in the same figure. The roughness scale experiences a strong variation along the LW surface supporting at strong winds the stress modulation. The model is capable of reproducing the laboratory measurements by *Miller and Shemdin* [1991] and shows that the main source of the observed SW modulation comes from the surface stress modulation.

[37] *Hara and Plant* [1994] presented estimates of the hydrodynamic MTF at VV polarization (the incidence angle is  $45^\circ$ ) extracted from field microwave radar measurements. The hydrodynamic MTF describes the variation of a microwave return along a LW profile caused by the modulation of the SW spectrum at the Bragg wave number  $k_b$ . In the notation of the present paper the hydrodynamic MTF is defined as  $M(k_b)$  (equation (24)). Compiled data of the amplitude and the phase of the hydrodynamic MTF from the work of *Hara and Plant* [1994, their Figure 7] as a function of the wind speed are plotted in Figure 8 together with model results. Frequencies of the observed LWs are in the range of  $0.25 < f < 0.3125$  Hz and the Bragg wave number  $k_b$  is  $277 \text{ rad m}^{-1}$ . Model results are for a LW of 0.3 Hz frequency.

[38] According to measurements the amplitude of the radar MTF increases with decreasing of the wind speed and the Bragg wave is enhanced on the LW crest. *Hara and Plant* [1994] showed that at moderate and strong winds their experimental estimates of the MTF contradict the expected behavior of the MTF based on the relaxation model (our reference runs) that predicts the suppression of the SW modulation at high winds and the shift of the MTF

phase toward the LW forward slope. They suggested that the modulation of the surface stress can be the mechanism, which provides the observed SW modulation. The model calculations for the Bragg wave MTF, the stress and roughness scale MTF are shown in Figure 8 together with corresponding reference runs. At low wind speeds the SW modulation is governed by the straining mechanism (the relaxation parameter is small). A large magnitude of  $|M(k_b)|$  results from the large value of  $d(\ln N)/d(\ln k)$  caused by a fast drop of the spectrum in the vicinity of  $k \sim k_\gamma$  due to the increasing role of viscous dissipation at low winds. At the wind speed exceeding  $10 \text{ m s}^{-1}$  the relaxation parameter is large and the SW modulation at the Bragg wave number is governed by the surface stress as suggested by *Hara and Plant* [1994]. Comparing the amplitude of the SW spectrum MTF and the stress MTF it is apparent that at high wind speeds they are almost equal  $|M(k_b)| \simeq |M_\tau|$ . The enhancement of SWs takes place at the LW crest, where the surface stress has the maximum.

[39] In Figure 9 the amplitude and the phase of the hydrodynamic MTF retrieved from K-band radar MTF (VV polarization, incidence angle is  $45^\circ$ ) are shown. This MTF relates to capillary waves and was obtained by *Kudryavtsev et al.* [2001b] (the radar wavelength is 0.8 cm, the Bragg wavelength is 0.7 cm) in the range of the modulating LW frequency  $0.15 \div 0.35$  Hz, and by *Grodsky et al.* [1999] (the radar wavelength is 1.2 cm, the Bragg wavelength is 0.85 cm) in the range of the modulating LW frequencies  $0.15 \div 0.4$  Hz. In both data sets bars indicate the standard deviation of the amplitude and the phase of the MTF from their mean value. Bragg scattering waves in these experiments are well inside the capillary range. Measurements show that the amplitude  $|M(k_b)|$  strongly increases with decreasing of the wind speed and that the enhancement of capillary waves occurs at the LW crests. The model calculation of the MTF for the 0.7 cm Bragg wave modulated by a LW with the frequency 0.25 Hz (corresponding to the mean observed LW frequency) is plotted in Figure 9. The model results are in a good agreement with observations. In this case Bragg waves relate to parasitic capillaries, and the source of their modulation is the cascade mechanism of energy transfer

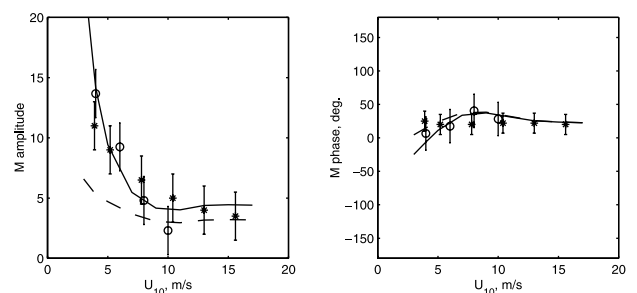


**Figure 9.** Amplitude and phase of the hydrodynamic MTF as a function of wind speed. Open circles: data compiled from the work of *Grodsky et al.* [1999]; stars: data compiled from the work of *Kudryavtsev et al.* [2001b]; error bars represent the standard deviation. Model calculations, solid line: MTF for the Bragg wave wavelength 0.7 cm; dashed line: MTF for the short gravity wave generating the Bragg wave. The LW frequency is 0.25 Hz.

from breaking gravity waves. The modulation of the short gravity wave at  $k = k_g$  results in the modulation of the rate of generation of parasitic capillaries at the wave number  $k = k_g^2/k_g$ . The MTF of the short gravity wave, which generates the Bragg parasitic capillary, is shown in Figure 9 by the dashed line. At low wind speeds the amplitude  $|M(k_b)|$  for capillary waves is amplified  $(n(k_g) + 1)$ -times in comparison with  $|M(k_g)|$  as it follows from equation (28). For the given case the amplification factor is equal to  $(n(k_g) + 1) = 2.8$  and explains the high modulation of capillary waves at low wind speeds. With increasing wind speed, the amplification factor reduces approximately to  $(n(k_g) + 1)/2$  according to equation (29). Since the enhancement of the generating gravity wave occurs at the LW crest the parasitic capillaries are also enhanced at the LW crest.

## 5. Impact of Coupled Dynamics on the LW Growth Rate

[40] In the previous section we have analyzed the influence of a LW on SWs and the aerodynamical property of the LW profile. The modulation of the sea drag is directly related to the roughness scale variation along the LW profile. It was shown that the amplitude of the LW-induced roughness scale variation is very strong so that one can anticipate a significant impact of varying roughness on the airflow dynamics and consequently on the wind growth rate of the modulating LW. A significant impact of varying roughness on the wind wave growth rate parameter was demonstrated by *Gent and Taylor* [1976] and *Maat and Makin* [1992]. In these studies the variation of roughness along the LW profile was arbitrary specified. In the present study it is found from the coupled airflow–SW model.

[41] To investigate the impact of varying roughness on the wave growth a simplified model of the turbulent airflow above waves by *Kudryavtsev et al.* [2001a] is used. The main simplification in the model was achieved by the division of the turbulent airflow into the outer ( $z > l$ ) and the inner region ( $z < l$ ), where the scale of the IR  $l$  is defined by (30). As it was already mentioned, the undulation of the airflow in the OR is close to inviscid. In particular, the horizontal velocity variation in the OR is described by equation (34). In the IR the dynamics of the wave-induced motion is significantly affected by the turbulent stress. The description of the IR dynamics is based on the solution of the equation for the shear stress [*Kudryavtsev et al.*, 2001a, equation (49)]. Accounting for the variation of the surface roughness in the model requires the modification of the lower boundary condition for the horizontal velocity. Just above the wave surface the wind velocity profile is locally logarithmic (36). At the surface  $z = \bar{z}_0$  it reads

$$\hat{u}_1(\bar{z}_0) = \hat{u}_s - \frac{\bar{u}_*}{\kappa} \frac{\hat{z}_0}{\bar{z}_0} \cos\varphi, \quad (41)$$

where  $\hat{z}_0$  is defined by (32) from the solution of the coupled airflow–SW model. When roughness is constant  $\hat{u}_1(\bar{z}_0)$  matches the LW orbital velocity at  $z = \bar{z}_0$ , while in the case of varying roughness the wind velocity matches  $\hat{u}_s$  at height  $z = \bar{z}_0 + \hat{z}_0 \exp i(Kx - \Omega t)$ .

[42] Figure 10 illustrates the model calculations of the LW-induced undulation of the horizontal and vertical veloc-

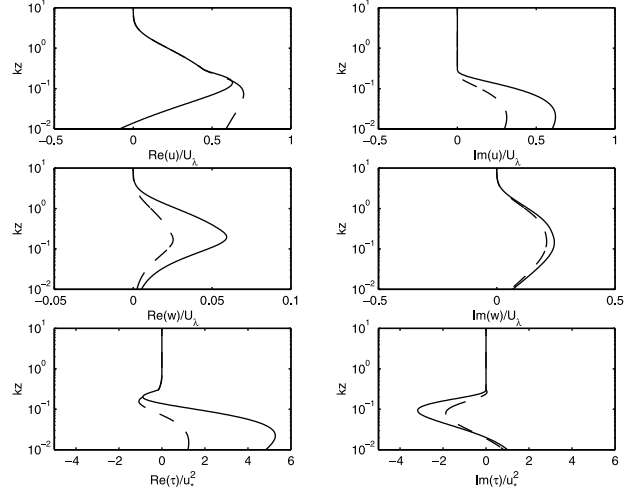


**Figure 10.** Vertical profiles of real and imaginary parts of the LW-induced variation; upper panels: horizontal velocity, middle panels: vertical velocity, lower panels: shear stress. Solid line: calculations with varying surface roughness; dashed line: calculations with constant surface roughness.

ity and the shear stress in the airflow in the case of constant and varying roughness. The inverse wave age parameter of the LW is  $U_{10}/C = 3$ , and the wind speed is  $U_{10} = 10 \text{ m s}^{-1}$ . The corresponding modulation of the SW spectrum is shown in Figure 3 and of the aerodynamical roughness in Figure 5. As it follows from Figure 5 the roughness scale MTF is large  $|M_{z_0}| \simeq 15$ , and its enhancement occurs on the LW crest. The model calculations of the turbulent airflow over the LW with varying surface roughness is presented in Figure 10. They show that the varying  $z_0$  significantly affects the vertical structure of all perturbations in the airflow induced by the LW. The magnitude of the turbulent stress variation is increased four to five times in comparison with the case of constant roughness. The real part of the vertical velocity undulation responsible for the energy transfer from wind to wave (equations (43) and (45) below) increases twice that should result in the increase of the energy transfer to the LW.

[43] The growth of the wave energy  $E_w$  due to energy transfer from wind to wave and due to the SWs modulation is described by equation

$$\frac{\partial E_w}{\partial t} = \rho_a c \left\langle P \frac{\partial \zeta}{\partial x} \right\rangle + \langle \tau u_s \rangle + \left\langle S_{11}^w \frac{\partial u_s}{\partial x_1} \right\rangle, \quad (42)$$

where  $E_w = 1/2 \rho_w g A^2$  is energy of the long gravity wave,  $P(z_0)$  is the surface pressure including the normal turbulent stress,  $\tau(z_0)$  is the turbulent stress, which equals the sum of the viscous surface stress and the form drag supported by SWs,  $S_{11}^w$  is the component of the SW radiation stress tensor, and brackets denote the horizontal averaging over the wavelength. It follows from (42) that the impact of SW on the LW growth rate is realized through the modulation of the form drag (accounted for in the second term on the right-hand side) and by the work of the radiation stress (third term) [*Kudryavtsev*, 1994]. The SW radiation stress is defined by *Phillips* [1977] as  $S_{\alpha\beta}^w = 1/2 \int l_{\alpha\beta} \omega N(\mathbf{k}) d(\mathbf{k})$ , where  $\alpha, \beta = 1, 2$ ; and  $l_{\alpha} = k_{\alpha}/k$ .

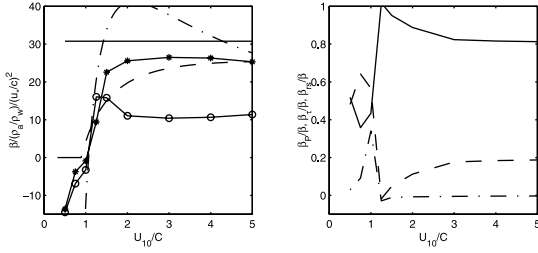


**Figure 11.** Wind wave growth rate parameter as a function of inverse wave age, left panel. Solid line marked by open circles: calculations with constant surface roughness; solid line marked by stars: calculations with varying surface roughness; solid line: empirical relation by *Plant* [1982]; dashed line: relation by *Stewart* [1974]; dashed-dotted line: empirical relation by *Snyder et al.* [1981]. Relative contribution of different mechanisms to the growth rate parameter, right panel. Solid line: work of the surface pressure; dashed line: work of the surface stress; dashed-dotted line: work of the wave radiation stress.

[44] The dimensionless growth rate parameter  $\beta$  is defined as

$$\beta = \frac{1}{E_w \omega} \frac{\partial E_w}{\partial t}.$$

In terms of the MTF and (42) this equation takes the form

$$\beta = \frac{\rho_a}{\rho_w} \frac{\bar{u}_*^2}{c^2} [Im(M_p) + Re(M_\tau) + Im(M_s)], \quad (43)$$

where  $M_p = \hat{P}/(KA\bar{u}_*^2)$  describes the energy flux due to the work of pressure on the vertical orbital velocity,  $M_\tau = \hat{\tau}/(KA\rho_a\bar{u}_*^2)$  describes the work of the surface stress on the horizontal orbital velocity, and  $M_s$  describes the work of the SW radiation stress on the gradient of the LW horizontal orbital velocity. The radiation stress is related to the SW spectrum MTF  $M(\mathbf{k})$  as

$$M_s = \frac{1}{2} \frac{\rho_w}{\rho_a} \frac{K}{\bar{u}_*^2} \int_{\varphi} \int_{k > k_{mod}} \cos^2 \varphi c^2 k^{-1} B(\mathbf{k}) M(\mathbf{k}) d\varphi d\ln k. \quad (44)$$

The surface pressure in (43) is determined by the profile of the vertical velocity and the shear stress

$$Im(\hat{P}) = \kappa^{-2} K \int_{z_0}^{\infty} (URe(\hat{w}) - Re(\hat{\tau}_{13})) dz. \quad (45)$$

The profile of  $\hat{w}(z)$  and  $\hat{\tau}_{13}(z)$  results from the solution of the model by *Kudryavtsev et al.* [2001a].

[45] The model calculations of the growth rate parameter (43) for the case of constant and varying surface roughness are shown in Figure 11. The empirical relation proposed by *Plant* [1982] (equation (6)) where  $C_\beta = 32$ , by *Snyder et al.* [1981] where  $\beta = 0.25(U_5/C - 1)$ , and the relation suggested by *Stewart* [1974] are shown as well. When the surface roughness is constant the model significantly underestimates the observed estimates. This fact was mentioned by numerous authors and is often thought as a result of non adequate modeling of turbulence above waves. However, the better understanding of turbulence above waves and the use of advanced turbulence closure schemes do not neces-

sary lead to better agreement between model results and measurements. For example, a simple mixing length closure scheme applied to the description of the IR with the assumption of the inviscid airflow undulation in the OR [*Belcher and Hunt*, 1993; *Kudryavtsev et al.*, 2001a] provides the same magnitude of the growth rate parameter  $\beta$  that is obtained by a numerical model by *Mastenbroek et al.* [1996] based on a second order closure scheme, both considerably underestimating observations.

[46] Accounting for varying surface roughness, which results through the modulation of SWs by a LW and the modulation of the stress, significantly increases the growth rate parameter. In the range of slow LWs ( $U_{10}/C > 2$ )  $\beta$  is amplified more than twice, and the model growth rate parameter moves closer to empirical estimates. For the fast LWs the effect of varying roughness does not affect the growth rate parameter. To illustrate the role of different mechanisms responsible for the LW growth rate the ratio of three terms in equation (43) to the total growth rate is shown in Figure 11. In the range of the inverse wave age parameter  $U_{10}/C > 1$  the work of the surface pressure determines the LW growth, while in the range  $0.5 < U_{10}/C \leq 1$  the work of the surface pressure and the surface stress has the same magnitude. The work of the SW radiation stress is negligible and this mechanism can be ignored in the wind wave growth problem.

[47] The varying surface roughness affects the growth rate of the LW by changing the structure of the IR modifying the velocity and the Reynolds stress profiles (Figure 10). The surface stress directly affects the growth rate (equation (43)) and it governs the dynamics of the IR. The wave-induced variation of the stress generates the slope-correlated component of the horizontal velocity, which in turn via the continuity equation causes the elevation-correlated component of the vertical velocity. According to equation (45) this component generates the slope-correlated pressure providing the energy transfer from wind to wave. This is so-called nonseparated sheltering mechanism, the most plausible mechanism of wind waves generation [*Belcher and Hunt*, 1993; *Kudryavtsev et al.*, 2001a]. The varying surface roughness enhances the undulation of the shear stress, correspondingly the undulation of the velocity components, and finally the growth rate parameter of the LW.

[48] The present model reduces considerably the discrepancy between modeled and observed estimates of the growth rate parameter. When the roughness scale variation induced by a LW through the modulation of SWs and the surface stress is accounted for the model estimates of the growth rate parameter become comparable with observations. It is important to notice that the variation of the roughness scale along the LW profile was not specified arbitrarily. It follows from the solution of the airflow–SW coupled model, which was verified on the basis of available measurements.

[49] Notice that our coupled model predicts much stronger impact of the varying surface roughness on the LW growth rate than that might be expected from the simplest parameterization of  $z_0$  via the Charnock relation. In this case the roughness scale MTF is  $M_{z_0} = 2M_*$  and as follows from (38) its effect on the surface stress MTF is small (of order  $\ln^{-1}(l/z_0) = 0.1$ ). Hence, the effect of varying roughness on the LW growth rate under these conditions is small, as was argued by *Belcher and Hunt* [1993].

## 6. Summary and Conclusions

[50] In the coupled sea surface–atmosphere model by *Kudryavtsev and Makin* [2001] the sea drag is provided by the viscous surface stress and the form drag. The form drag is realized by the momentum flux to regular surface waves described in terms of the wind wave growth parameter and by the momentum flux due to the airflow separation from breaking waves. At moderate and strong winds the form drag dominates the sea drag. Most of the form drag is supported by high frequency part of the wave spectrum. Hence, the dominant LWs modulating SWs can significantly affect the turbulent airflow above.

[51] The model was extended here to provide the description of the coupled modulation of SWs (in the range from capillary to gravity waves) and modulation of the form drag (written in terms of the roughness scale variation) induced by a LW. In the gravity and capillary gravity range the modulation of SWs results from the wave straining and the action of the LW-induced variation of the wind surface stress. The modulation of short gravity waves, which generate parasitic capillaries, provides a strong modulation in the capillary range. The variation of the wind surface stress is described by the dynamics of the turbulent airflow over the LW with varying surface roughness. Varying surface roughness results from SWs modulations supporting the form drag of the sea surface. The main contribution to the modulation of the surface roughness comes from wave breaking, which is strongly modulated by dominant waves. Field measurements by *Dulov et al.* [2002] showed that the amplitude of the whitecap coverage exceeds by 25 times the steepness of the modulating LW. This result is confirmed by the present model. The modulation of SWs, of the surface roughness and of the turbulent stresses are all coupled, which provides a feedback in the airflow–SW system in the presence of a LW.

[52] Model calculations are in a good agreement with laboratory and field measurements by *Miller and Shemdin* [1991], *Hara and Plant* [1994], *Grodsky et al.* [1999], and *Kudryavtsev et al.* [2001b] who studied the modulation of capillary and capillary gravity waves by LWs. The relaxation model, which only takes into account the straining mechanism of the SW modulation, significantly underestimates the measurements.

[53] The model results showed that the amplitude of the surface roughness scale variation along the LW can be very large. In terms of the MTF it can reach values of 10–20. The variation in the roughness scale considerably affects the dynamics of the turbulent airflow over the LW and thus the LW wind growth rate. Models of the airflow above waves assuming constant roughness underestimate the growth rate parameter approximately by two to three times as compared to the measured values. The present study showed that when the variation in the surface roughness is accounted for, the growth rate parameter increases roughly twice considerably reducing the discrepancy with measurements. It is important to notice that the variation in the roughness scale is not imposed arbitrarily in the model but results from the self-consistent solution of the coupled airflow–SW system disturbed by a long gravity wave.

[54] **Acknowledgments.** This research was supported by the Office of Naval Research (ONR grants N00014-98-1-0437 and N00014-98-1-

0653 and PR grants 98PR04572-00 and 98PR05889-00) and partly by the Netherlands Organization for Scientific Research (NWO) through the Dutch–Russian Scientific Cooperation Programme 2001, project 047.014.009. V. N. Kudryavtsev also acknowledges support from the Norwegian Space Center (Contract JOP.8.3.3.06.01.2).

## References

- Alpers, W. R., and K. Hasselmann, The two-frequency microwave technique for measuring ocean-wave spectra from an airplane or satellite, *Boundary Layer Meteorol.*, **13**, 215–230, 1978.
- Belcher, S. E., and J. C. R. Hunt, Turbulent shear flow over slowly moving waves, *J. Fluid Mech.*, **251**, 109–148, 1993.
- Cox, C. S., and W. H. Munk, Statistics of the sea surface derived from sun glitter, *J. Mar. Res.*, **13**, 198–227, 1954.
- Dulov, V., V. Kudryavtsev, and A. Bol'shakov, A field study of white caps coverage and its modulations by energy containing waves, in *Gas Transfer at water surfaces*, edited by M. A. Donelan et al., pp. 187–192, AGU, Washington, D. C., 2002.
- Gent, P. R., and P. A. Taylor, A numerical model of the airflow above water waves, *J. Fluid Mech.*, **77**, 105–128, 1976.
- Grodsky, S. A., V. N. Kudryavtsev, A. N. Bol'shakov, and V. E. Smolov, A field study of wave-induced variations in the radar signal, *Mor. Gidrofiz. Z.*, **4**, 26–40, 1999.
- Hara, T., and W. J. Plant, Hydrodynamic modulation of short wind-wave spectra due to long waves measured by microwave radar, *J. Geophys. Res.*, **99**, 9767–9784, 1994.
- Kudryavtsev, V. N., The coupling of wind and internal waves: Modulation and friction mechanism, *J. Fluid Mech.*, **278**, 33–62, 1994.
- Kudryavtsev, V. N., and V. K. Makin, The impact of airflow separation on the drag of the sea surface, *Boundary Layer Meteorol.*, **98**, 155–171, 2001.
- Kudryavtsev, V. N., C. Mastenbroek, and V. K. Makin, Modulation of wind ripples by long surface waves via the air flow: A feedback mechanism, *Boundary Layer Meteorol.*, **83**, 99–116, 1997.
- Kudryavtsev, V. N., V. K. Makin, and B. Chapron, Coupled sea surface atmosphere model, 2, Spectrum of short wind waves, *J. Geophys. Res.*, **104**, 7625–7639, 1999.
- Kudryavtsev, V., D. Hauser, G. Caudal, and B. Chapron, Semiempirical model of the normalized radar cross section of the sea surface, I, The background model, *J. Geophys. Res.*, **107**, doi:10.1029/2001JC001003, in press, 2002.
- Kudryavtsev, V. N., V. K. Makin, and J. F. Meirink, Simplified model of the airflow above waves, *Boundary Layer Meteorol.*, **100**, 63–90, 2001a.
- Kudryavtsev, V. N., V. V. Malinovskii, A. N. Bol'shakov, and V. E. Smolov, A field study of mechanisms of the radar scattering modulations by surface waves, *Issled. Zemli Kosm.*, **4**, 13–30, 2001b.
- Maat, N., and V. K. Makin, Numerical simulation of airflow over breaking waves, *Boundary Layer Meteorol.*, **60**, 77–93, 1992.
- Makin, V. K., V. N. Kudryavtsev, and C. Mastenbroek, Drag of the sea surface, *Boundary Layer Meteorol.*, **73**, 159–182, 1995.
- Mastenbroek, C., V. K. Makin, M. H. Garat, and J. P. Giovanangeli, Experimental evidence of the rapid distortion of turbulence in the airflow over water waves, *J. Fluid Mech.*, **318**, 273–302, 1996.
- Miller, S. J., and O. H. Shemdin, Measurements of the hydrodynamic modulation of centimetre waves, *J. Geophys. Res.*, **96**, 2749–2759, 1991.
- Phillips, O. M., *The Dynamics of the Upper Ocean*, 336 pp., Cambridge Univ. Press, New York, 1977.
- Phillips, O. M., Spectral and statistical properties of the equilibrium range in the wind-generated gravity waves, *J. Fluid Mech.*, **156**, 505–531, 1985.
- Plant, W. J., A relationship between wind stress and wave slope, *J. Geophys. Res.*, **87**, 1961–1967, 1982.
- Romeiser, R., A. Schmidt, and W. Alpers, A three-scale composite surface model for the ocean wave-radar modulation transfer function, *J. Geophys. Res.*, **99**, 9785–9801, 1994.
- Snyder, R. L., F. W. Dobson, J. A. Elliott, and R. B. Long, Array measurements of atmospheric pressure fluctuations above surface gravity waves, *J. Fluid Mech.*, **102**, 1–59, 1981.
- Stewart, R. W., The air–sea momentum exchange, *Boundary Layer Meteorol.*, **6**, 151–167, 1974.
- Townsend, A. A., Flow in a deep turbulent boundary layer over a surface distorted by water waves, *J. Fluid Mech.*, **55**, 719–735, 1972.
- Yelland, M., and P. K. Taylor, Wind stress measurements from the open ocean, *J. Phys. Oceanogr.*, **26**, 541–558, 1996.

V. N. Kudryavtsev, Marine Hydrophysical Institute, Kapitanskaya 2, 335000 Sevastopol, Ukraine. (odmi@alpha.mhi.iuf.net)

V. K. Makin, Royal Netherlands Meteorological Institute, P.O. Box 201, 3730 AEDe Bilt, Netherlands. (makin@knmi.nl)